

Kinetic Study of the Water-Gas Shift Reaction at Ultralow Temperature over a Ru-Based Supported Ionic Liquid Phase Catalyst

Ferdinand Fischer* and Andreas Jess

DOI: 10.1002/cite.202200052

 This is an open access article under the terms of the Creative Commons Attribution License, which permits use, distribution and reproduction in any medium, provided the original work is properly cited.



Supporting Information
available online

The water-gas shift reaction is subject to thermodynamic limitation, i.e., CO conversion increases with decreasing temperature. Thus, it is preferential to keep temperatures as low as possible at reasonable kinetic rates. In this work, the performance of a ruthenium-based supported ionic liquid phase catalyst is shown for the water-gas shift reaction at ultralow temperature. Furthermore, a model for the intrinsic kinetics of the water-gas shift reaction using this supported ionic liquid phase catalyst is presented. For this purpose, a formal kinetic power law and a mechanistic general catalytic cycle kinetic approach were applied. Supported ionic liquid phase catalysts with filling levels up to 30 % were prepared. For filling levels < 13 %, internal mass transport limitations do not occur and intrinsic kinetics prevail.

Keywords: Ru-based catalysts, Supported ionic liquid phase, Water-gas shift reaction

Received: May 03, 2022; *revised:* June 24, 2022; *accepted:* August 01, 2022

1 Introduction

As fossil fuel-based energy production, in line with nuclear power, is going to be substituted by renewable energy sources, the interest in green hydrogen production rises steadily. Growing markets for decentralized and mobile power generation based on fuel cells application in transport or heating units will probably lead to a huge demand for hydrogen [1,2]. Currently, green hydrogen production by electrolysis covers only 2 % of the worldwide demand, 1.9 % as by-product of Cl-alkali electrolysis and even only 0.1 % by water electrolysis [3]. Thus, industrial hydrogen production will rely on current synthesis routes mainly based on fossil fuels such as natural gas in the near future until large-scale water electrolysis driven by renewables (wind, PV, etc.) will take over. The existing natural gas network makes methane available nearly everywhere where it is desired. Thus, the steam reforming process is a promising hydrogen source for decentral or mobile applications, at least in Europe. For both applications, the polymer electrolyte membrane fuel cell (PEMFC) is the standard fuel cell, due to moderate operating temperatures (80 °C) and the associated dynamic mode of operation [2]. However, carbon monoxide (CO) is formed in the steam reforming process (10–13 vol %) leading to deactivation of the Pt electrode of the PEMFC due to strong adsorption of CO [4]. Thus, the CO concentration in the feed gas has to be lower than

10 ppm for Pt electrodes and below 250 ppm for PtRu alloy electrodes, respectively [5]. For the removal of CO, the water-gas shift (WGS) reaction is used.



The WGS produces additional hydrogen, thereby increasing the overall hydrogen balance. In addition, the catalysts are unaffected by CO₂. As shown in Eq. (1), the water-gas shift reaction is exothermic, i.e., low operating temperatures are preferred to yield a high equilibrium conversion of CO (Fig. 1). An alternative to WGS for reduction of the CO content is catalytic preferential CO oxidation, but it is out of the scope of this work to discuss this process in more detail.

Regarding the above mentioned decentralized and mobile hydrogen supply of fuel cells by means of steam reforming and subsequent water-gas shift purification, WGS catalysts should operate at the lowest possible temperatures (ultralow temperature WGS; $T < 180$ °C). In addition, the catalysts

Ferdinand Fischer, Prof. Dr.-Ing. Andreas Jess
ferdinand1.fischer@uni-bayreuth.de
University of Bayreuth, Department of Chemical Engineering,
Center of Energy Technology, Universitätsstraße 30, 95447 Bayreuth, Germany.

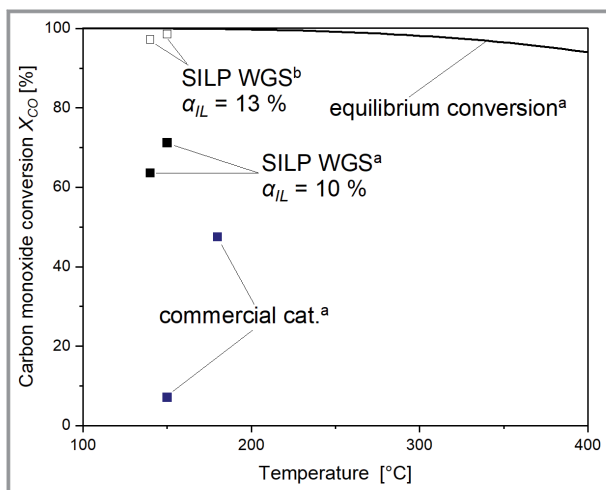


Figure 1. Carbon monoxide conversion of different catalysts at ultralow temperature compared to the thermodynamic equilibrium conversion determined by the chemical reaction and equilibrium software HSC Chemistry, which is using the Gibbs energy minimization method. A thermodynamic database “HSC Thermochemical Database” is stored in the software, whereby excerpts can be found in Sect. S10 of the Supporting Information. The conversion data of the commercial catalyst^a and the SILP WGS^b catalyst are from the work of Werner et al. [6]. The SILP WGS^b catalyst was prepared and tested in this work. a) $m_{\text{cat}} = 0.2 \text{ g}$, $w_{\text{cat}} = 0.02 \text{ g}_{\text{cat}}\text{g}_{\text{support}}^{-1}$, $p_{\text{total}} = 300 \text{ kPa}$, steam/syngas ratio = 3:1, 75 % H_2 , 8 % CO , 13 % CO_2 , 4 % N_2 , $GHSV = 12000 \text{ h}^{-1}$; b) $m_{\text{SILP}} = 8 \text{ g}$, $w_{\text{cat}} = 0.016 \text{ g}_{\text{cat}}\text{g}_{\text{support}}^{-1}$, $p_{\text{total}} = 100 \text{ kPa}$, 10 % CO , 60 % N_2 , 30 % H_2O , $\dot{V}_{\text{total}} = 7.5 \text{ L}_{\text{N}}\text{h}^{-1}$.

should be able to start up and shut down dynamically without loss of activity. With regard to these requests, supported ionic liquid phase (SILP) catalysts show a promising performance compared to commercially used WGS catalysts ($\text{CuO}/\text{ZnO}/\text{Al}_2\text{O}_3$) [6].

SILP catalysts are made of a (highly) porous (inert) solid that contains the homogeneous catalyst dissolved in an ionic liquid and has been applied successfully in hydroformylation [7]. In addition, in SILP catalysis, the ionic liquid can also act as the homogeneous catalyst. Hence, SILP catalysts combine the advantages of heterogeneous and homogeneous catalysis: the homogeneous catalyst dissolved in an ionic liquid (IL) is immobilized on a heterogeneous porous support particle with a large surface area. In addition, the IL remains on the inner surface due to the extremely low vapor pressure. Therefore, the homogeneous catalyst is permanently dissolved, as loss of solvent (IL) during the reaction due to evaporation can be neglected. Thus, the SILP system offers a decisive advantage over supported liquid phase (SLP) catalysts [8, 9]. As the catalysts are homogeneous in nature, good to excellent activity as well as selectivity occurs at mild operating parameters (temperature, pressure), and the separation of catalyst from product is easy or even not needed in case of a fixed bed. Werner et al. [10, 11] identified a ruthenium-based catalyst dissolved in the ionic liquid [BMMIM][Cl] as the most promising WGS-SILP catalyst.

The activity of this catalyst exceeds the activity of commercial catalysts at low temperatures. According to Werner et al. [6], the CO conversion with the SILP catalyst is ten times higher at 150 °C compared to the commercially used catalyst at real gas compositions (Fig. 1). Fig. 1 also shows a ruthenium-based SILP catalyst system yielding CO conversion of almost 100 %. Hence, precision cleaning as in the methanation process by preferential oxidation or pressure swing adsorption might not be required [12]. In addition, SILP catalysts are characterized by very good dynamic behavior in comparison with commercial catalysts, i.e., hardly no activity loss at one shut-down and start-up cycle. Fig. 2 shows the result of a shut-down and start-up cycle of a SILP catalyst measured in this work. In fact, the commercial catalyst is destroyed by condensed water during the shutdown [4].

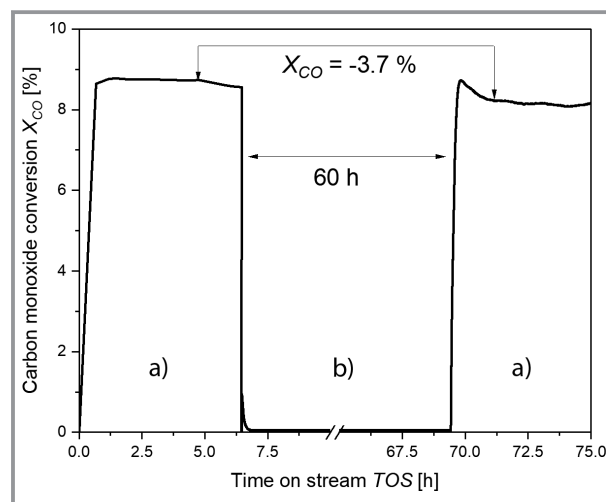


Figure 2. Dynamic behavior of the WGS-SILP catalyst in a shut-down and start-up cycle measured in this work: $T_{\text{reactor}} = 120 \text{ }^\circ\text{C}$, $m_{\text{SILP}} = 2 \text{ g}$, $\dot{V}_{\text{total}} = 18 \text{ L}_{\text{N}}\text{h}^{-1}$, $\alpha_{\text{IL}} = 0.18$, $\zeta = 0.67$, $p_{\text{total}} = 1 \text{ bar}$. a) $p_{\text{CO}} = 0.1 \text{ bar}$, $p_{\text{H}_2\text{O}} = 0.2 \text{ bar}$, $p_{\text{N}_2} = 0.7 \text{ bar}$; b) $p_{\text{CO}} = 0 \text{ bar}$, $p_{\text{H}_2\text{O}} = 0 \text{ bar}$, $p_{\text{N}_2} = 1 \text{ bar}$.

In this paper, the kinetic behavior of an optimized Ru-based SILP catalyst as developed by Werner et al. is presented [10]. This work contains the experimental results of the kinetic study of the SILP catalyst and an investigation and comparison of different approaches to describe the intrinsic kinetics. The knowledge of reaction kinetics is important for the optimal design of chemical reactors on a technical scale. In addition, the influence of the filling degree of the SILP catalysts with three different catalyst IL concentrations was also systematically studied. Furthermore, the effect of the catalyst loadings at constant IL filling degree was investigated. The resulting Ru offset was investigated and implemented in the intrinsic kinetics.

2 Experimental

2.1 Calculations

For a SILP catalyst, the pore filling degree is a crucial parameter. The degree of pore filling can be viewed from several perspectives (see Fig. 3). Thus, the filling level can refer to the ionic liquid (α_{IL} , Eq. (2)) located in the pore volume only or to the ionic liquid and the ruthenium catalyst (α_{syn} , Eq. (3)). Both parameters are adjustable during production. However, the pore filling degree during the reaction (α_{reac} , Eq. (4)) depends also on the reactants and products (mainly steam) dissolved in the IL catalyst solution, i.e., α increases during the time on stream (TOS).

$$\alpha_{IL} = \frac{V_{IL}}{V_{pore}} \quad (2)$$

$$\alpha_{syn} = \frac{V_{IL+Ru-complex}}{V_{pore}} \quad (3)$$

$$\alpha_{reac} = \frac{V_{IL+Ru-complex+educt+product}}{V_{pore}} \quad (4)$$

The pore filling degree of the IL was measured using the elemental analyzer EA 3000 (HEKAtech). Thereby, the nitrogen content of the SILP catalyst was determined. As the imidazolium ring of the ionic liquid is the only part containing nitrogen, the IL content can be calculated. This

method agreed with reference measurements from BET and TGA analysis.

The ratio of the molar amounts of ruthenium to IL is represented by ζ :

$$\zeta = \frac{n_{Ru}}{n_{IL}} \quad (5)$$

The ruthenium content was determined via inductively coupled plasma-optical emission spectrometry (ICP-OES) using the ICP-OES Optima 7300 DV (PerkinElmer).

Since the amount of side products formed is extremely low ($S_{CO_2} \approx 100\%$), the carbon mass balance is given accurately by Eq. (6):

$$\dot{n}_{CO,in} = \dot{n}_{CO,out} + \dot{n}_{CO_2,out} \quad (6)$$

Therefore, CO conversion is calculated using Eq. (7).

$$X_{CO} = \frac{\dot{n}_{CO,in} - \dot{n}_{CO,out}}{\dot{n}_{CO,in}} \quad (7)$$

Because of the differential operation (gradientless) of the reactor at low conversions ($< 15\%$), Eq. (8) holds for calculating the reaction rates.

$$r_{CO} = \frac{X_{CO}\dot{n}_{CO,in}}{m_{support}} = \frac{X_{CO}\dot{V}_{CO,in}p_{CO}}{m_{support}RT} \quad (8)$$

As the catalysts investigated contained different amounts of active components and, thus, had different filling degrees, the rate is always related to the mass of support instead of the total catalyst mass. In this way, the Ru offset, i.e., the amount of Ru not active for catalysis (explained in more detail in Sect. 3.2) is easily incorporated in the rate equation.

2.2 Kinetic Approach

In the present work, two different kinetic rate approaches were applied to describe the homogeneously catalyzed reaction kinetics. First, a simple power law approach, i.e., a formal kinetic approach, is used, where m , n , l , q , and j are reaction orders (Eq. (9)):

$$r = k(T) \left(p_{CO}^m p_{H_2O}^n - p_{CO_2}^l p_{H_2}^q \right) \left(\frac{n_{Ru}}{m_{support}} \right)^j \quad (9)$$

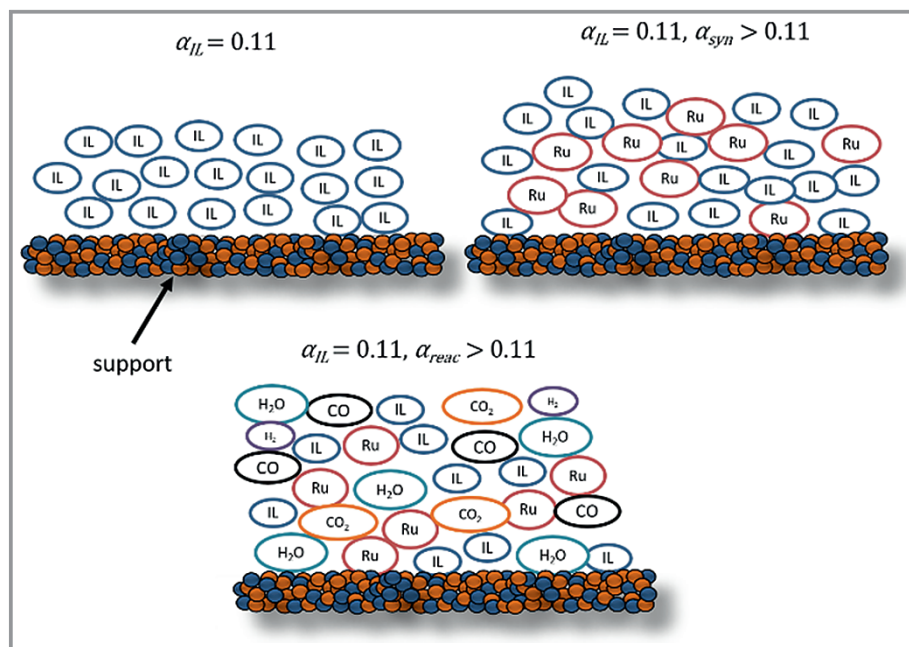


Figure 3. Graphical representation of the pore filling degrees α_{IL} , α_{syn} , and α_{reac} with [BMMIM][Cl] as IL and Ru complexes as Ru.

The reaction order of the catalyst concentration (j) is assumed to be $j = 1$. By introduction of the molar amount of ruthenium to the mass of the support, Eq. (9) takes the form of an effective rate equation, in agreement with Eq. (8). At conversions below 15 %, the reaction is in the differential region, consequently, the backward reaction, i.e., the reverse water-gas shift reaction (RWGS), can be neglected. At such low conversions, the partial pressures can be expressed as

$$p_{\text{CO}} \approx p_{\text{CO},\text{in}} \quad p_{\text{H}_2\text{O}} \approx p_{\text{H}_2\text{O},\text{in}} \quad p_{\text{CO}_2} \approx 0, \quad p_{\text{H}_2} \approx 0 \quad (10)$$

Now, the kinetic approach simplifies to

$$r = k(T) p_{\text{CO}}^m p_{\text{H}_2\text{O}}^n \frac{n_{\text{Ru}}}{m_{\text{support}}} \quad (11)$$

$k(T)$ is the temperature-dependent reaction rate constant, which is given according to Arrhenius:

$$k(T) = k_0 \exp\left(-\frac{E_A}{RT}\right) \quad (12)$$

For homogeneously catalyzed reactions, mechanistic kinetic approaches are possible and are applied. In this study, the general catalytic cycle kinetics (GCCCK) method developed by Christiansen [13, 14] and established by Helfferich [15, 16] and Murzin and Salmi [17] is used. For this method, a mechanistically established catalytic cycle has to be assumed. Stepić et al. [18] proposed a catalytic cycle of the WGS reaction with Ru-based SILP catalysts that is shown in Fig. 4.

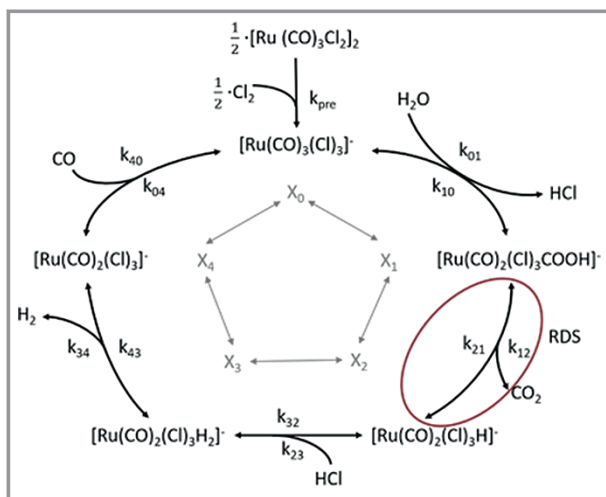


Figure 4. Catalytic cycle of Ru-based SILP WGS reaction proposed by Stepić et al. [18]. In an upstream reaction, which already takes place during the SILP production, two active anionic Ru complexes (X_0) are formed from a ruthenium dimer precursor, whereby a chloride ion of the ionic liquid coordinates to each Ru central atom. As a result, the active Ru complex, with three chloride and three CO ligands each, becomes the anionic part of the ionic liquid.

The following GCCCK rate equation has been developed and has been used for modeling the reaction kinetics of the WGS reaction with Ru-based SILP catalyst; Eq. (13) was derived according to the procedure described in Sect. S8 of the Supporting Information, starting from the catalytic cycle shown in Fig. 4.

$$r = \frac{k_1 \exp\left(-\frac{E_A}{RT}\right) p_{\text{CO}} p_{\text{H}_2\text{O}}}{1 + K_2(T) p_{\text{CO}} + K_3(T) p_{\text{CO}} p_{\text{H}_2\text{O}}} \frac{n_{\text{Ru}}}{m_{\text{support}}} \quad \text{with} \quad (13)$$

$$K_i(T) = k_i \exp\left(\frac{-\Delta H_i}{RT}\right)$$

It has to be noted that the temperature-dependent constants in the inhibition term are not adsorption equilibrium constants as in heterogeneous catalysis, but constants that describe the complexation of the reactants to the active Ru complex.

2.3 Modeling and Parameter Estimation

While the formal kinetic approach can be solved by linearization of the Arrhenius equation, the GCCCK approach requires a numeric least-square method to determine the necessary parameters; this was performed in Matlab (solver `fmincon`). The optimized parameters of the nonlinear regression are determined by minimizing the objective function (OF), i.e., the normalized sum of the residual squares.

$$OF = \sum_{i=1}^{n_{\text{exp}}} \left(\frac{y_{\text{cal}} - y_{\text{exp}}}{y_{\text{exp,max}}} \right)^2 \quad (14)$$

The two parameters of the Arrhenius (k_1 and E_A) or complexation equation (k_2/k_3 and $\Delta H_2/\Delta H_3$) show a strong correlation. To reduce this correlation in the regression step, the reparametrized form of the equation with an expansion of a mean temperature (T_m) is used [19].

$$k_1 \exp\left(-\frac{E_A}{RT}\right) = k_m \exp\left(\frac{-E_A}{R} \left(\frac{1}{T} - \frac{1}{T_m}\right)\right) \quad (15)$$

The quality of the fit is determined with the root-mean-square error ($RMSE$) or the coefficient of determination (R -squared) values.

$$RMSE = \sqrt{\frac{1}{n_{\text{exp}}} \sum_{i=1}^{n_{\text{exp}}} (y_{\text{calc}} - y_{\text{exp}})^2} \quad (16)$$

$$R^2 = 1 - \frac{\sum_{i=1}^{n_{\text{exp}}} (y_{\text{exp}} - y_{\text{cal}})^2}{\sum_{i=1}^{n_{\text{exp}}} (y_{\text{exp}} - \bar{y}_{\text{cal}})^2} \quad (17)$$

The smaller the $RMSE$ values and the closer the R^2 values are to 1, the better the model fits the experimental data.

A reasonable comparison between different models can be performed using the F test that is used to test the adequacy and global significance of models, according to Eq. (18).

$$F = \frac{\sum_{i=1}^{n_{\text{exp}}} y_{\text{exp}}^2}{\frac{p}{\sum_{i=1}^{n_{\text{exp}}} (y_{\text{cal}} - y_{\text{exp}})^2}} \quad (18)$$

A model is considered globally significant if the calculated F values are greater than the tabulated F values at the selected significance level and the given degrees of freedom $F_{(p, n_{\text{exp}} - p)}$. The global significance of a model is regarded as reliable when the F values are greater than 100 [20]. The advantage of this comparison is that the number of parameters of the models is used for validation.

3 Results

3.1 Pseudo-Intrinsic SILP Catalyst Kinetics

Intrinsic kinetics describe the reaction path without consideration of mass and heat transport. Thus, the measurement of intrinsic kinetics (microkinetic) requires preparation of a “pseudo-intrinsic catalyst” that has no restriction of mass transport. In the SILP system, mass transport limitations can occur due to pore diffusion limitation or mass transport limitation in the liquid phase. As the catalyst particles used are very small ($d_{\text{particle}} = 1 \text{ mm}$) and a filling ratio of 11% was applied, pore diffusion limitation can be neglected (see Sect. S5 in the Supporting Information). Mass transport limitations in the liquid phase are neglected if the reaction rate increases linearly with rising pore filling degree. This is due to the fact that at a constant ζ value, the amount of active ruthenium complexes increases proportionally with the increase of the pore filling degree of the system. As shown in Fig. 5, the intrinsic range is located between 8 and 13% ($\zeta = 0.67$) pore filling degree. A pore filling degree of 11% was chosen for “intrinsic” α . From a filling level of 13% upwards, the reaction rate deviates from linearity; however, at 15% filling level, a plateau appears because mass transport limitation occurs at a higher filling level. The apparent decrease in the reaction rate after the plateau is due to the catalyst run-in time (see Sects. S6 and S7 in the Supporting Information). The smaller the molar ratio of ruthenium to IL, the further the graph shifts to higher filling levels and the steeper the slope and the smaller the plateau become. This is caused by the fact that, at the same α_{IL} values, the catalysts with lower ζ contain lower amounts of active component.

Apart from the filling degree, the effect of catalyst loading on the intrinsic kinetics has to be investigated. At a constant pore filling degree of $\alpha_{\text{IL}} = 0.11$, i.e., without mass transport limitation, the SILP system is in the intrinsic regime if the reaction rate increases linearly with rising ruthenium

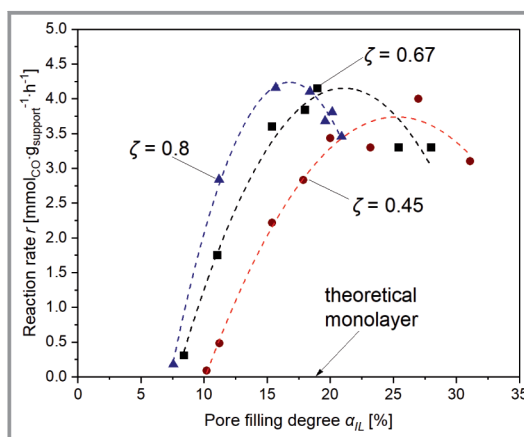


Figure 5. Reaction rate vs molar pore filling degree α_{IL} at three different ζ at $TOS = 20 \text{ h}$. The determination of the theoretical monolayer is shown in Sect. S3 of the Supporting Information. $T_{\text{reactor}} = 120 \text{ }^\circ\text{C}$, $m_{\text{support}} = 1.9 \text{ g}$, $V_{\text{total}} = 18 \text{ L N h}^{-1}$, $p_{\text{total}} = 1 \text{ bar}$, $p_{\text{CO}} = 0.1 \text{ bar}$, $p_{\text{H}_2\text{O}} = 0.2 \text{ bar}$, $p_{\text{N}_2} = 0.7 \text{ bar}$.

amount. In a standard homogeneously catalyzed system, the reaction rate would start to increase linearly as soon as a ruthenium complex is part in the SILP system. However, in the SILP system investigated in this paper, a certain number of Ru complexes are required before a reaction occurs. Hoffmeister et al. [21] have described and discussed this phenomenon for SLP systems. There are several ways to explain the loss of active material: 1) The inner surface of the support has adsorption sites that show high affinity to ruthenium complexes. These Ru complexes rendered inactive for catalysis. 2) The SILP catalyst is drawn into the micropores of the support by capillary forces. This happens in particular if the mobility of the Ru complex-IL system is increased by water adsorption during the reaction. This effect is described by Strobel [22] and Werner [10] and in more detail in Sect. S6 of the Supporting Information. Hoffmeister et al. [21] and Redondo de Beloqui [23] assume that active complexes are sterically hindered in the micropores and, therefore, are unable to catalyze the reaction of reactants entering the micropore. 3) The liquid phase consisting of IL and active centers floods the micropores as in 2). Thus, the interface between the liquid-gas phase becomes small and is limited to the area at the pore entrance. A low diffusion rate of the reactants in the liquid phase having a maximum of around $10^{-9} \text{ m}^2 \text{ s}^{-1}$ [24–26] results, therefore, in mass transport limitation. 4) The ruthenium content of the non-active ruthenium species in the system has to be considered [27]. However, the true reason for the ruthenium offset is still unclear and requires further research. Apart from the Ru offset, the rate grows linearly for ruthenium contents between $\zeta = 0.45$ and 0.8 (Fig. 6). At higher molar ruthenium amounts ($\zeta > 0.8$), the slope of the reaction rate decreases until a drop in the reaction rate occurs. This is caused by the fact that mass transport limitation takes effect at higher filling levels α_{syn} . Furthermore, at higher ζ , the amount of chloride provided by the IL may no

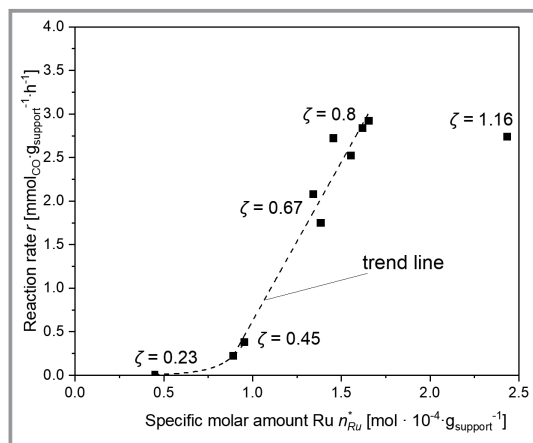


Figure 6. Reaction rate vs specific molar amount of Ru at constant filling degree at $TOS = 7$ h. $\alpha_{IL} = 0.11 = \text{constant}$, $d_{\text{particle}} = 1$ mm, $T_{\text{reactor}} = 120$ °C, $m_{\text{support}} = 1.9$ g, $\dot{V}_{\text{total}} = 18$ L_N h⁻¹, $p_{\text{total}} = 1$ bar, $p_{\text{CO}} = 0.1$ bar, $p_{\text{H}_2\text{O}} = 0.2$ bar, $p_{\text{N}_2} = 0.7$ bar.

longer be sufficient to convert all ruthenium dimers present in the IL into the active Ru species (see Sect. S9 of the Supporting Information).

3.2 Consideration of the Ru Offset in the Reaction Rate Approaches

Both reaction kinetic approaches described in Sect. 2.2 assume that each ruthenium atom is part of a catalytically active complex. However, this assumption leaves the Ru offset explained in Sect. 3.1 unconsidered. Therefore, the kinetic approaches must be revised with regard to the Ru offset. Consequently, the molar amount of the ruthenium offset has to be subtracted from the total ruthenium amount.

$$r = k_1 \exp\left(\frac{-E_A}{RT}\right) p_{\text{CO}}^m p_{\text{H}_2\text{O}}^n \frac{n_{\text{Ru}} - n_{\text{Ru off}}}{m_{\text{support}}} \quad \text{with} \quad n_{\text{Ru off}} = n_{\text{Ru off}}^* m_{\text{support}} \quad (19)$$

$$r = \frac{k_1 \exp\left(\frac{-E_A}{RT}\right) p_{\text{CO}}^m p_{\text{H}_2\text{O}}^n}{1 + k_2 \exp\left(\frac{-\Delta H_2}{RT}\right) p_{\text{CO}} + k_3 \exp\left(\frac{-\Delta H_1}{RT}\right) p_{\text{CO}} p_{\text{H}_2\text{O}}} \times \frac{n_{\text{Ru}} - n_{\text{Ru off}}}{m_{\text{support}}} \quad (20)$$

At steady-state operation ($TOS = 110$ h) and in the intrinsic kinetic range ($\alpha_{IL} = 0.11$), the Ru offset is obtained by linear extrapolation of the reaction rates of the catalysts ($\zeta = 0.67$) onto the abscissa. Referring the offset to the mass of the support allows for an easy transfer to and comparison with other catalysts. For $\zeta = 0.67$, the specific Ru offset ($n_{\text{Ru off}}^*$) for the used support is $1.14 \cdot 10^{-4}$ mol_{Ru}g_{support}⁻¹.

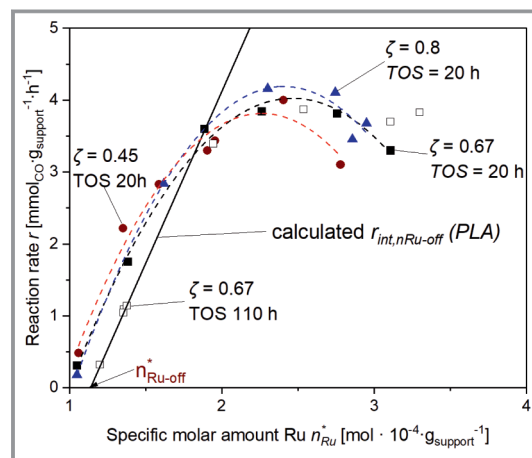


Figure 7. Reaction rate vs specific molar amount of Ru for three different ζ and varying filling degree. $T_{\text{reactor}} = 120$ °C, $m_{\text{SILP}} = 2-4$ g, $\dot{V}_{\text{total}} = 12-18$ L_N h⁻¹, $p_{\text{total}} = 1$ bar, $p_{\text{CO}} = 0.1$ bar, $p_{\text{H}_2\text{O}} = 0.2$ bar, $p_{\text{N}_2} = 0.7$ bar.

From Fig. 7, it can be concluded that the amount of IL has little effect on the reaction rate when based on the support mass at lower filling degrees. Comparing the rates at $1 \cdot 10^{-4}$ and $1.3 \cdot 10^{-4}$ mol_{Ru}g_{support}⁻¹, it can be assumed that the Ru offset becomes only slightly smaller with decreasing ζ . The maximum rate is reached at a molar Ru amount of about $2.4 \cdot 10^{-4}$ mol_{Ru}g_{support}⁻¹ for each ζ . Above this ruthenium content, the reaction rate remains approximately constant. Deviating from this, the measuring points at $TOS = 20$ h show a decrease due to the run-in time (see Sect. S6 of the Supporting Information). However, further studies are needed to determine effective kinetics.

3.3 Intrinsic Kinetics

The partial pressure variation of CO and H₂O yield their reaction orders for the power law approach (Fig. 8a). The resulting orders for water and carbon monoxide are 0.82 and 0.15, respectively. The reaction order with respect to water is significantly higher since the water molecules play a decisive role in the rate-determining step of the catalytic cycle [18]. Due to these results, a simplified power law approach with integer orders of 1 for H₂O and 0 for CO is also considered. The activation energy ($E_A = 63.1$ kJ mol⁻¹) and the pre-exponential factor (Tab. 1) are obtained by linearization of Eq. (11) (Fig. 8b). All values are in good agreement with already determined values by SILP-WGS catalysts [10, 22].

Optimization of the GCCK approach with six fitting parameters results in a much lower activation energy of about 39 kJ mol⁻¹ compared with E_A obtained by linearization of the power law approach. Consequently, the temperature dependence of the complexation equilibria constants is overestimated in this model. When the possible parameter range of the activation energy is fixed around the value

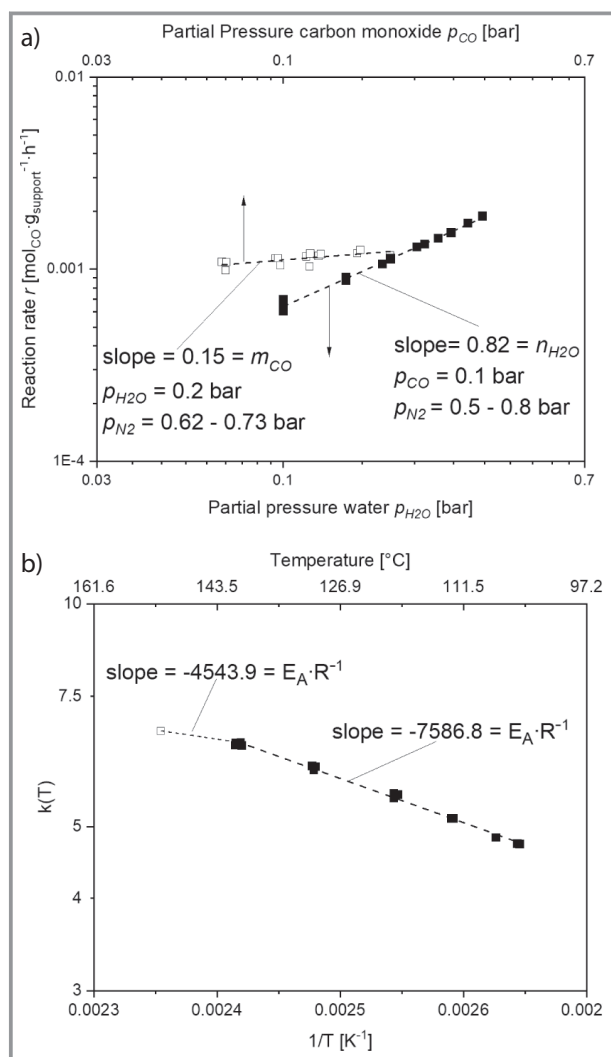


Figure 8. a) Reaction rate as a function of partial pressure of water or carbon monoxide. $T_{\text{reactor}} = 120$ °C, $m_{\text{SILP}} = 4$ g, $\dot{V}_{\text{total}} = 12$ L_N h⁻¹, $p_{\text{total}} = 1$ bar. b) Arrhenius plot, $k(T)$ as a function of the reciprocal temperature between 105 and 151 °C for power law approach with orders for water and carbon monoxide of 0.82 and 0.15, respectively. $T_{\text{reactor}} = 105$ – 151 °C, $m_{\text{SILP}} = 4$ g, $\dot{V}_{\text{total}} = 12$ L_N h⁻¹, $p_{\text{total}} = 1$ bar, $p_{CO} = 0.1$ bar, $p_{H_2O} = 0.2$ bar, $p_{N_2} = 0.7$ bar.

Table 1. (Fit) parameter of the different approaches.

Parameter	Power law approach	Simplified power law approach	GCCK approach	Simplified GCCK approach
m_{CO} [-]	0.82	0	1	1
n_{H_2O} [-]	0.15	1	1	1
k_1 [bar ^{-(m+n)} h ⁻¹]	$6.2 \cdot 10^{10}$	$5.8 \cdot 10^{10}$	$2.7 \cdot 10^{12}$	$5 \cdot 10^{12}$
E_A [kJ mol ⁻¹]	63.1	63	61.8	64.2
K_2 [bar ⁻¹]	-	-	48.1	50.8
K_3 [bar ⁻²]	-	-	59.4	0

obtained from the linearization, the temperature dependence of the complexation equilibrium almost completely disappears. Therefore, the temperature-dependent constants in the inhibition term were replaced by temperature-independent constants in the GCCK approach; thereby, the number of adjustable parameters is reduced to 4. The temperature-independent constants (K_2 and K_3) were determined using isothermal regression. For this purpose, the model parameters were based on 31 individual measurement points at 120 °C. In the second step, a non-isothermal regression was performed to determine the activation energy and the pre-exponential factor (k_1). To avoid falsification of the model due to the different weighting of the temperatures, the same number of measured values was used at each temperature. The activation energy for the GCCK approach resulting from the parameter estimation (shown in Tab. 1) is in good agreement with the activation energy obtained by linearization. To further simplify the model (SGCCK), the parameter K_3 was set to 0, since the complexation of CO contributes the most to the inhibition of the reaction rate. CO complexation inhibits the reaction rate 5 times more than the combined complexation of CO and H₂O.

The parity plots of the four different approaches are shown in Fig. 9. All parity plots show that the applied kinetic models match the experimental values very well (Fig. 9). Considering R^2 and $RMSE$, all models are in the same quality range. When the number of fitting parameters is included in the qualitative evaluation by the F test, the power law approaches (Figs. 9a and b) are superior to the mechanistic ones. The F values of all models indicate global significance. The model with integer reaction orders (Fig. 9b) shows satisfactory results. However, a slight dependence of the reaction rate on CO can be seen in this parity plot since the minor rate changes during CO variation are not included. In the considered CO partial pressure range of 0.07 to 0.18 bar, the resulting error is still comparatively small ($\pm 10\%$). When extrapolating to partial pressures outside this range, the error gets larger and the reaction order of CO should be considered. Therefore, the power law approach is assumed to be the best model.

4 Conclusion

In this work, the influence of the filling ratio, the particle diameter, and the catalyst loading on the reaction rate of supported ionic liquid phase catalysts is investigated for the water-gas shift reaction. By means of the experimental data, catalyst parameters ($d_{\text{particle}} = 1$ mm, $\alpha_{IL} = 11\%$, and $\zeta = 0.67$) are selected at which the reaction kinetics are in the

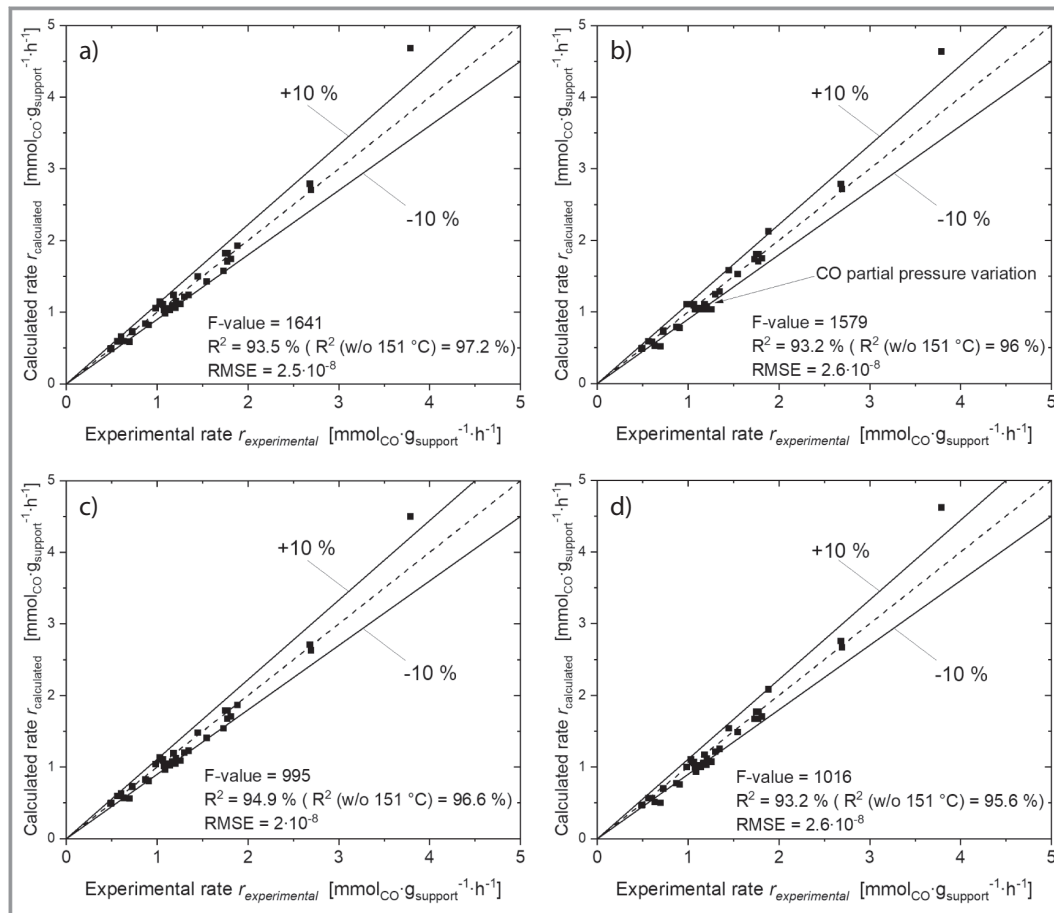


Figure 9. Parity plots for comparison of the four different intrinsic kinetic approaches: a) power law approach, b) simplified power law approach, c) GCKK, and d) SGCKK rate equations, with the error interval of $\pm 10\%$. $T_{\text{reactor}} = 105\text{--}151\text{ }^{\circ}\text{C}$, $m_{\text{SILP}} = 4\text{ g}$, $V_{\text{total}} = 12\text{ L}_N\text{ h}^{-1}$, $p_{\text{total}} = 1\text{ bar}$, $p_{\text{CO}} = 0.07\text{--}0.18\text{ bar}$, $p_{\text{H}_2\text{O}} = 0.1\text{--}0.4\text{ bar}$, $p_{\text{N}_2} = 0.5\text{--}0.8\text{ bar}$.

intrinsic range. Intrinsic kinetics are measured using this pseudo-intrinsic catalyst. Subsequently, the experimentally determined values are used to develop mathematical models. Two formal kinetic power law approaches and two mechanistic approaches are used. It is shown that the intrinsic kinetics of the SILP-WGS catalysts can be represented very well with all four approaches, where the power law approach shows the best fit with the highest F value.

Supporting Information

Supporting Information for this article can be found under DOI: <https://doi.org/10.1002/cite.202200052>. This section includes additional references to primary literature relevant for this research [28–30].

Open access funding enabled and organized by Projekt DEAL.

Symbols used

d	[m]	diameter
E_A	[J mol ⁻¹]	activation energy
ΔH_i	[J mol ⁻¹]	complexation energy
ΔH_R	[J mol ⁻¹]	standard reaction enthalpy
$k(T), K(T)$	[various]	temperature-dependent constants
K	[various]	temperature-independent constant
k_1	[bar ^{-(m+n)} h ⁻¹]	pre-exponential factor
m	[g]	mass
\dot{m}	[g h ⁻¹]	mass flow
n	[mol]	molar amount
n^*	[mol g ⁻¹]	specific molar amount
\dot{n}	[mol h ⁻¹]	molar flow
p	[Pa]	partial pressure
r	[mol g _{Ru complex} ⁻¹ h ⁻¹]	reaction rate

R^2	[%]	coefficient of determination (R-squared)
RMSE	[-]	root-mean-square error
S	[-]	selectivity
T	[°C, K]	temperature
TOS	[h]	time on stream
\dot{V}	[L ³ h ⁻¹]	volume flow
X	[-]	conversion

Greek letters

α	[%]	filling degree
ζ	[-]	molar ratio of ruthenium to IL

Sub- and superscripts

Al ₂ O ₃	aluminum oxide
CO	carbon monoxide
CO ₂	carbon dioxide
H ₂	hydrogen
H ₂ O	water
IL	ionic liquid
Pt	platinum
Ru	ruthenium

Abbreviations

BET	Brunauer-Emmett-Teller
GA	gas analyzer
GCCK	general catalytic cycle kinetics
OF	objective function
RWGS	revers water-gas shift
SGCCK	simplified general catalytic cycle kinetics
SILP	supported ionic liquid phase
SLP	supported liquid phase
TGA	thermogravimetric analysis
WGS	water-gas shift

References

- [1] R. Farrauto, S. Hwang, L. Shore, *Annu. Rev. Mater. Res.* **2003**, *33*, 1–27. DOI: <https://doi.org/10.1146/annurev.matsci.33.022802.091348>
- [2] J. Zalc, M. Löffler, *J. Power Sources* **2002**, *111*, 58–64. DOI: [https://doi.org/10.1016/S0378-7753\(02\)00269-0](https://doi.org/10.1016/S0378-7753(02)00269-0)
- [3] A. Jess, P. Wasserscheid, *Chemical Technology*, 2nd ed., Wiley-VCH, Weinheim **2020**.
- [4] A. Platon, Y. Wang, *Hydrogen and Syngas Production and Purification Technologies*, (Eds: K. Liu, C. Song, V. Subramani), John Wiley & Sons, Hoboken, NJ **2009**.
- [5] J. Divisek, H.-F. Oetjen, V. Peinecke, *Electrochim. Acta* **1998**, *43* (24), 3811–3815. DOI: [https://doi.org/10.1016/S0013-4686\(98\)00140-6](https://doi.org/10.1016/S0013-4686(98)00140-6)
- [6] S. Werner, N. Szesni, M. Kaiser, *ChemCatChem* **2010**, *2* (11), 1399–1402. DOI: <https://doi.org/10.1002/cctc.201000245>
- [7] J. M. Marinkovic, A. Riisager, R. Franke, P. Wasserscheid, M. Hauman, *Ind. Eng. Chem. Res.* **2019**, *58* (7), 2409–2420. DOI: <https://doi.org/10.1021/acs.iecr.8b04010>
- [8] A. Riisager, R. Fehrmann, M. Hauman, *Eur. J. Inorg. Chem.* **2006**, *2006* (4), 695–706. DOI: <https://doi.org/10.1002/ejic.200500872>
- [9] J. Villadsen, H. Livbjerg, *Catal. Rev.: Sci. Eng.* **1978**, *17* (1), 203–272. DOI: <https://doi.org/10.1080/03602457808080882>
- [10] S. Werner, Ultra-Low Temperature Water–Gas Shift Reaction with Supported Ionic Liquid Phase (SILP) Catalysts, *Ph.D. Thesis*, Friedrich-Alexander-Universität Erlangen-Nürnberg, Erlangen **2011**.
- [11] S. Werner, N. Szesni, A. Bittermann, *Appl. Catal., A* **2010**, *377* (1–2), 70–75. DOI: <https://doi.org/10.1016/j.apcata.2010.01.019>
- [12] D. B. Pal, R. Chand, S. N. Upadhyay, *Renewable Sustainable Energy Rev.* **2018**, *93*, 549–565. DOI: <https://doi.org/10.1016/j.rser.2018.05.003>
- [13] J. A. Christiansen, *Z. Phys. Chem.* **1935**, *28B* (1), 303–310. DOI: <https://doi.org/10.1515/zpch-1935-2828>
- [14] J. A. Christiansen, *Adv. Catal.* **1953**, *5*, 311–353. DOI: [https://doi.org/10.1016/S0360-0564\(08\)60644-6](https://doi.org/10.1016/S0360-0564(08)60644-6)
- [15] F. G. Helfferich, *J. Phys. Chem.* **1989**, *93*, 6676–6681. DOI: <https://doi.org/10.1021/j100355a022>
- [16] F. G. Helfferich, *Kinetics of Homogeneous Multistep Reactions*, 1st ed., Comprehensive Chemical Kinetics, Vol. 38, Elsevier, Amsterdam **2001**.
- [17] D. Y. Murzin, T. Salmi, *Catalytic Kinetics Chemistry and Engineering*, 2nd ed., Elsevier, Amsterdam **2016**.
- [18] R. Stepić, C. R. Wick, V. Strobel, *Angew. Chem.* **2019**, *131* (3), 751–755. DOI: <https://doi.org/10.1002/ange.201811627>
- [19] M. Schwaab, J. C. Pinto, *Chem. Eng. Sci.* **2007**, *62*, 2750–2764. DOI: <https://doi.org/10.1016/j.ces.2007.02.020>
- [20] K. Toch, J. W. Thybaut, G. B. Martin, *AIChE J.* **2015**, *61* (3), 880–892. DOI: <https://doi.org/10.1002/aic.14680>
- [21] M. Hoffmeister, D. Hesse, *Chem. Ing. Sci.* **1990**, *45* (8), 2575–2580. DOI: [https://doi.org/10.1016/0009-2509\(90\)80144-4](https://doi.org/10.1016/0009-2509(90)80144-4)
- [22] V. Strobel, Towards Rational Design of SILP Catalysts: A Water-Gas Shift Reaction Case Study, *Ph.D. Thesis*, Friedrich-Alexander-Universität Erlangen-Nürnberg, Erlangen **2020**.
- [23] M. S. Redondo de Beloqui, Einfluss der Porenstruktur auf das Umsatzverhalten von “Supported Liquid-Phase”-Katalysatoren, *Ph.D. Thesis*, Universität Hannover **1989**.
- [24] I. Reche, I. Gallardo, G. Guirado, *RSC Adv.* **2014**, *4*, 65176–65183. DOI: <https://doi.org/10.1039/C4RA11297K>
- [25] M. Shokouhi, H. Sakhaeinia, H. Jalili, *J. Chem. Thermodyn.* **2019**, *133*, 300–311. DOI: <https://doi.org/10.1016/j.jct.2019.02.022>
- [26] C. Moya, J. Palomar, M. Gonzalez-Miquel, *Ind. Eng. Chem. Res.* **2014**, *53* (35), 13782–13789. DOI: <https://doi.org/10.1021/ie501925d>
- [27] T. Bauer, R. Stepić, P. Wolf, *Catal. Sci. Technol.* **2018**, *8*, 344–357. DOI: <https://doi.org/10.1039/C7CY02199B>
- [28] H. Livbjerg, B. Sorensen, J. Villadsen, in *Chemical Reaction Engineering – II*, Advances in Chemistry Series, Vol. 133, American Chemical Society, Washington, D.C. **1974**, 242–258. DOI: <https://doi.org/10.1021/ba-1974-0133.ch019>
- [29] B. Romanovsky, I. G. Tarkhanova, *Russ. Chem. Rev.* **2017**, *86* (5), 444–458. DOI: <https://doi.org/10.1070/RRCR4666>
- [30] P. Savage, *Educ. Chem. Eng.* **2008**, *42* (4), 211–217.